Dynamic Cognitive States Predict Individual Variability in Behavior and Modulate with EEG Functional Connectivity during Working Memory

Christine Beauchene[a,b,e], **Thomas Hinault**[c,e,f], **Sridevi V. Sarma**[a,b,e,*], **and Susan Courtney**[a,c,d,e,*]

[a]Institute for Computational Medicine; [b]Biomedical Engineering; [c]Psychological and Brain Sciences; [d]Neuroscience; [e]Johns Hopkins University; [f]U1077 INSERM-EPHE-UNICAEN; [*]Co-Senior Author

This manuscript was compiled on August 9, 2021

Short-term fluctuations in strategy, attention, or motivation can cause large variability in cognitive performance across task trials. Typically, this variability is treated as noise when analyzing the relationships among behavior, neural activity, and experimentally structured task rules and stimuli. These relationships are thought to remain consistent over repeatedly administered identical task conditions (e.g. trial types and stimuli) while the variability is assumed to be random and to cancel out when averaged across trials and individuals. We propose that the variability carries important information regarding a participant's internal cognitive states, and could provide insights into both intra- and inter-individual differences in performance and its neural bases. However, these states are difficult to quantify, as they are not directly measurable. Therefore, we use a mathematical, state-space modeling framework to estimate internal cognitive states from measured behavioral data to predict each participant's reaction time fluctuations. We can quantify each participant's sensitivity to different factors (e.g. previous performance or distractions) that were predicted to affect cognitive states, and thus become sources of variability. By including a participant's states in the behavioral model, we improved model performance by a factor of 10, over a model with only experimental task parameters. We show how the participant-specific states reflect neural activity by identifying EEG functional connectivity features that modulate with each state. Overall, this approach could better quantify and characterize both individual and population behavioral differences across time, which could improve understanding of the neural mechanisms underlying the interactions among cognitive, strategic and motivational processes affecting behavior.

Internal Cognitive State | State-Space Models | Working Memory | EEG | Functional Connectivity

Identifying the neural underpinnings of working memory (WM), the ability to actively maintain and use task-relevant information (1–3), or any other cognitive process, requires identifying a relationship between the experimentally structured task rules and stimuli, and the generated neural and behavioral responses. Generally, these relationships are thought to remain consistent when identical task conditions (i.e. trial types and stimuli) are repeatedly administered over a session.

This is often not the case, however, because even within a set of identical task trials, large differences can exist in recorded brain activity (e.g. magnitude, neuroanatomical location) and behavior (responding faster or slower, correctly or incorrectly). Such variability can be observed both between participants, and within a single participant during a session. The conventional assumption is that variability within an individual in both neural and behavioral responses is a consequence of noise. However, a growing trend in cognitive science is the belief that spontaneous neural activity contains valuable information (4–6). In this study, we build upon these ideas and argue that variability within individuals may be attributed to factors that are not random noise, but which are also not directly observable or easily predictable, such as fluctuations in attention or motivation. In addition, each of these factors may be more or less influential on one individual's behavior versus another's.

For example, imagine various scenarios where such cognitive/motivational states might affect your response on a cognitive task. If you are consistently answering correctly, then you might feel more confident or motivated, resulting in faster response times in present and future trials. On the other hand, a streak of incorrect answers may cause you to become more cautious and slower in order to learn from your mistakes. The opposite may be true as well, in that you may instead get frustrated with a losing streak and therefore speed up your response time. In addition, you may choose a different strategy from another individual performing the same task, or

Significance Statement

Cognitive neuroscience researchers attempt to control every aspect of experimental conditions, but differences in strategy, or fluctuations in attention and motivation often cannot be controlled or reliably measured. Such factors can produce highly variable behavior both across and within individuals, which may contain important information. We propose a mathematical modeling framework, using measured data to estimate a participant's dynamic, internal cognitive states, with each state derived from specific factors hypothesized to affect attention, motivation or strategy. The results highlight potential strategies, and reveal EEG features that modulate with each state. Our method quantifies and characterizes individual behavioral differences and highlights their underlying neural mechanisms, which could be used for future targeted training or neuromodulation therapies to improve cognitive performance.

S.C. conceived and planned the experiments. T.H. carried out the experiments. C.B. and S.V.S. designed the model and the computational framework and analysed the data. All authors contributed to the interpretation of the results. C.B. took the lead in writing the manuscript. All authors provided critical feedback and helped shape the research, analysis and manuscript.

None of the authors have competing interests.

[2]To whom correspondence should be addressed. E-mail: cbeauch2jhu.edu

you may change strategies as you learn more about the task demands. Such cognitive/motivational states can vary during a session. We refer to these short-term fluctuations that affect behavior as internal states, which are challenging to quantify because they are not directly measurable.

Internal states are reflected in neural activity, which may be an independent representation of the state or multiplexed with neural activity related to motor behavior or cognitive processes. Disentangling the motivational, behavioral, and cognition-related neural activation patterns is necessary for understanding how each state varies within and across individuals.

We used a dataset from a previous study (7) in which a salient, distracting stimulus was presented during the delay period of a spatial working memory task (8, 9). Overall, individual reaction times varied greatly in all participants within a single session. In the current study, we used a state-space modeling framework to estimate internal states from measured behavioral data, which characterized the highly variable reaction times recorded during a working memory task performed while electroencephalography (EEG) data were collected. Using the state-space model, we tested our hypothesis that reaction time is a function of the task, stimuli, noise, and *identifiable internal states*. We identified three internal states that significantly improved model performance. These states were related to the participant's recent past performance (including previous errors and reaction times), and to their previous susceptibility to distraction. By including these internal states in the behavioral model, the model performance improved by a factor of 10 and could reliably predict reaction time (RT) variability. We then performed a regression analysis to identify a set of EEG features that could predict the internal states.

Finally, we showed that we can substitute the internal states estimated from EEG features for the internal states derived from measured behavior to reliably predict reaction time variability from neural activity. We identified a small number of EEG features whose activity level directly correlated with the significance of the internal state to the prediction of RT. Specifically, we found that information regarding an individual's accuracy on preceding trials is related to right fronto-parietal connectivity and left parietal local activity in the gamma band. An individual's reaction time on preceding trials, on the other hand, is associated with left fronto-parietal connectivity in the gamma band and temporo-parietal connectivity in the alpha band. Finally, left frontal activity in the gamma band is linked with the effect of distractors on RT in previous trials.

While results are in line with previous work on top-down control of information processing (10) and attention control (11), our findings suggest that variability in working memory performance within and across individuals is due to more than task parameters, cognitive capacity, and noise. Previous studies have also found effects of past performance and distraction on future performance in group analyses. The results here, however, demonstrated that the degree to which each cognitive internal state, and its associated EEG features, contributed to the prediction of RT was different for each participant. In addition, each cognitive state (and thus its contribution to RT) also varied across time within individuals. Therefore, the results suggest this approach could be used to better quantify and characterize individual participants' differences in cognitive performance, their dynamics, and their underlying neural mechanisms.

Results

Reaction time is highly variable during a working memory task. In this study, we analyzed the behavioral and EEG data of 16 participants from a previously published study in our laboratory (7). The task involved remembering one of two different types of spatial information (spatial location or relation between items) across a delay period. During the delay, irrelevant stimuli briefly appeared on both the left and right side of fixation, with a more salient, previously rewarded distractor being either on the same (congruent) or opposite (incongruent) side as the subsequent working memory test stimulus (Fig 1, for more detail see Fig 8). Participants responded with a button press to indicate whether the test stimulus matched the

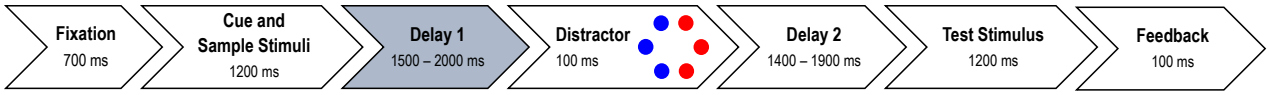

Fig. 1. Flowchart trial schematic showing the WM task and the shaded time period during which the EEG data was analyzed. For further details, refer to the methods section.

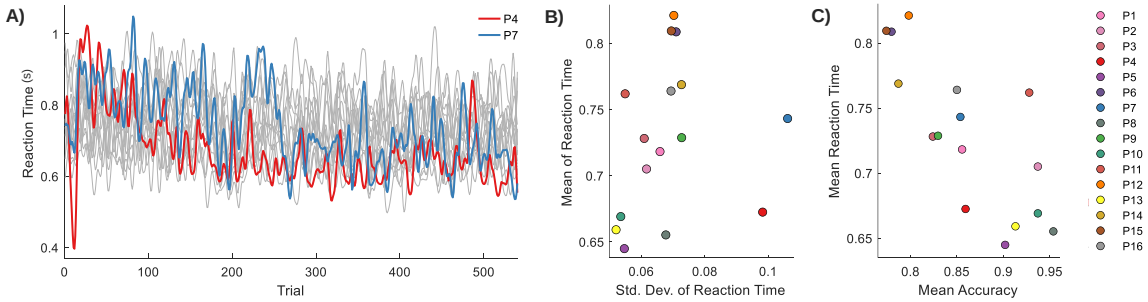

Fig. 2. A) RT time-series traces for all participants. Participant 4 (red) and Participant 7 (blue) are highlighted. B) A comparison of the mean and standard deviation of the RT, for all participants. C) A comparison of the mean task accuracy, and mean RT over all participants.

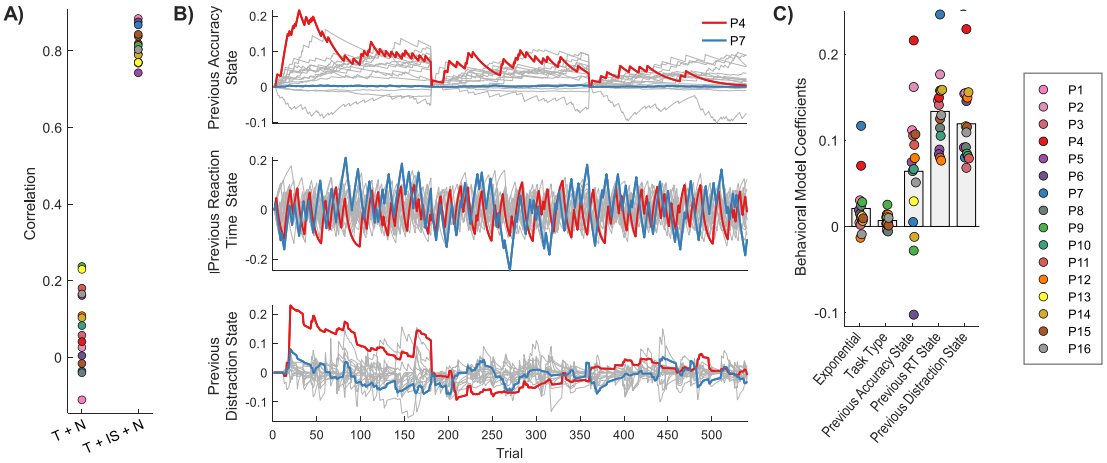

Fig. 3. A) A comparison of the testing dataset correlations for the two models. T = Task, IS = Internal States estimated from behavioral model, N = noise. B) Trajectories for each of the states, for all participants. The states are reset to 0 at trial 180 and 360 to account for breaks that occurred between task blocks. Participant 4 and Participant 7 are highlighted in red and blue, respectively. C) The fitted β's of each model term, for all participants.

remembered sample stimulus according to the relevant spatial dimension.

The reaction time (RT) varied not only between participants but also within a single participant across trials (Figure 2A). Overall, the RT time series showed the characteristic exponential decrease in RT, potentially reflecting learning of the task. Also, the high-frequency oscillations observed were hypothesized to have been due to stimulus differences across trials, noise, or latent variables correlated with motivation, attention, or confidence. A summary of the variation in mean and standard deviation of the RT time series over the different participants is displayed in Fig 2B. The mean accuracy (percentage of correct answers over the 540 trials) and the mean RT, for each participant, are shown in Fig 2C.

Dynamic internal states reliably predict trial-by-trial reaction time across participants. We first asked: "Can the observed highly variable reaction times be predicted with a model using only experimentally structured task rules and noise?" To answer the question, we used a general linear modeling (GLM) framework to develop participant-specific models to predict the RT (Eqn 2, Methods). We defined the model of RT to be a function of the task (T) and noise (N). Included in the task variables were four indicator functions (comprised of 0s and 1s) identifying the presented task type (location vs relation trial, see Methods), hemifield of the test stimuli (left vs right), and whether the hemifield of the distractor stimuli was congruent or incongruent with the hemifield of the test stimuli.

To identify the most important terms in the model, we compared the resulting fitted parameters for each model term, which included the weight in front of each term, β, and the associated p-value. If the p-value was less than 0.05, then the weight was considered to be significantly different from zero and contributed to the model prediction. Based on the model, we found the task type to be the most significant behavioral model term for predicting trial-by-trial RT in over 50% of participants. This was consistent with the previous work by our group on this dataset (7), which showed in a hypothesis-driven analysis that the RT was significantly shorter for location than relation trials, across trials and participants. However, the T + N model (Fig 3A) could not accurately capture the overall dynamics observed in the RT: Correlation (Mean $\pm$ SD): 0.07 ± 0.09.

Therefore, we next asked "Can internal cognitive states, in addition to task rules and noise, predict reaction time?" We incorporated a state-space modeling framework into the GLM to build dynamical models of past behavior for each of the participants. Previous work by our group had shown that internal states could accurately predict variations in behavior, such as risk-taking in a gambling task (12–14). Therefore, we referred to the new model, which included the task rules (T), the internal states (IS), and noise (N), as the T + IS + N model (Eqn 3, Methods). In order to reduce the complexity of the model, we chose to only include the task type indicator function (location vs relation) from the task variables, based on the results of the original model.

Briefly, the internal states captured different components of the participants' behavior and were generally defined as

$$\underbrace{x(t+1)}_{\text{state}} = \underbrace{ax(t)}_{\substack{\text{state}\\\text{memory}}} + \underbrace{u(t)}_{\substack{\text{task}\\\text{outcome}}} \qquad [1]$$

where the state, x, evolved over each trial (time step), t, by multiplying the current value of the state by a weight, a, which captured the contribution (or memory) of past task outcomes, u, to the current state value. The a's were identified individually for each participant, using a search grid. In particular, we defined three internal states to predict RT: 1) Previous Accuracy State (Eqn 4), 2) Previous RT State (Eqn 5), and 3) Previous Distraction State (Eqn 6). As shown in Fig 3A, by using the three states, task type, exponential decay, and noise, we could accurately capture each participant's RT time series with the model: Correlation (Mean $\pm$ SD): 0.81 ± 0.04).

- Previous Accuracy State: the state received a positive unit input pulse on each trial that a participant answered incorrectly. Therefore, the state only deviated from zero if the participant made an incorrect response. If a was small (close to 0), then, on an incorrect answer, the state increased by one (due to the input pulse) and quickly decayed back to zero. However, if a was large (close to 1), then, again, the

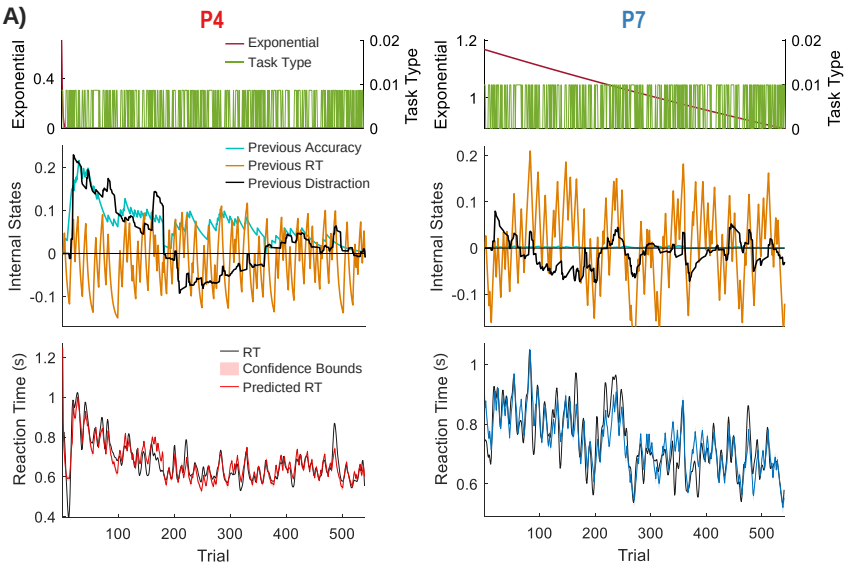

Fig. 4. A) The top panels show each term of the model (scaled by its respective β). The exponential for P4 decays quickly. The bottom two panels show the predicted RT from the model overlaid with the RT. B) A scatter plot comparing the RT to the predicted RT. The training and testing data points are denoted by the colored circles and colored diamonds outlined in black, respectively. The solid black line shows perfect correlation (i.e. the $y = x$ line)

state increased in amplitude by one, and slowly decayed back to zero over the subsequent trials. If the state had not fully decayed to zero by the next incorrect answer, then the state could accumulate those recent errors. If the fitted weight (β) from the behavioral model was positive, then, when the participant made an error, the state increased, and, as a result, the participant's RT increased (or slowed down). The opposite occurred if β was negative, then, an error caused the state to decrease, which resulted in RT decreasing.

- Previous RT State: a positive or negative unit input pulse was applied on each trial. The direction of the pulse was determined by the sign (positive or negative) of the difference between the RT of the current trial and the preceding trial. Therefore, the state accumulated information regarding the changing trend of the participants' RT over time. If the fitted weight was positive, then the state fluctuated in the same direction as the RT. For example, if the participant was getting faster over the previous two trials (i.e. a negative input), then the state decreased as well, and RT decreased. Alternatively, if the fitted weight was negative, the opposite occurred and the trend was flipped (i.e. as the state decreased, RT increased).

- Previous Distraction State: The purpose of this state was to quantify the difference in RT during trials where the previously rewarded distractor color was in the same hemifield (congruent) or opposite hemifield (incongruent) as the working memory test stimuli. This factor was previously associated with performance differences when averaging across trials and participants (7), but the magnitude of the effect of distraction varied both across participants and across trials within a participant. If a person continued to be affected by the distraction stimulus, then the "distraction" affected the congruent trials in the opposite direction as incongruent trials. For example, if a person's attention was attracted by the distractor and the test stimulus was presented in the same hemifield (congruent trial), then RT decreased because their focus did not need to shift to the other side of the screen. However, if their attention was attracted by the distractor and then the test stimulus appeared on the opposite side (incongruent trial), then RT increased. This effect disappeared as the participants learned to ignore the distractor (i.e. delearned the previous association), and thus the predicted effect of congruence on the current trial converged to zero.

  For this state, an input pulse only occurred on congruent or incongruent trials. We defined the input to be the difference in the RT on the latest congruent vs. latest incongruent trial. The direction of this effect, however, was opposite depending on whether the current trial was congruent or incongruent. Specifically, the operator in front of the input depended on the current trial type, subtraction (shorter RT) for congruent or addition (longer RT) for incongruent trials. Similar to the Previous RT State, the sign of the fitted weight indicated the direction of the state fluctuations in relation to RT.

Using this methodology, we developed participant-specific dynamical models to identify different components of the behavior. By using GLMs, we uncovered which terms of the model (Eqn 3) weighed the most into predicting RT, for each participant. The trajectories for each of the states (scaled by their respective β's) are shown for each person in Fig 3B. We chose to highlight Participant 4 and 7 throughout this analysis because they had similar accuracy and exhibited the largest variability in RT, but they weighted their internal states very differently.

Overall, the participants varied in which terms were weighted (β) the most in their respective models (Fig 3C). Across all participants, the Exponential weight was generally positive, resulting in a negative exponential trend, suggesting task learning. In addition, the Task Type (Location or Relation working memory) resulted in the smallest weights across all participants but was still a significant

model term in five participants. The weights of the internal states were generally larger than the weights associated with the other model terms (not including the constant: -0.44 ± 0.25).

The Past Accuracy State was generally positive, which showed that as the participant accumulated errors, their RT increased (participants were slower to respond). Only in three participants were the fitted weights negative, which showed the opposite trend occurred, where they responded faster with accumulated incorrect answers. In addition, all weights for the Previous RT State were positive, which suggested that the positive or negative RT trend over the previous two trials continued on the current trial. Finally, for the Previous Distraction State, all the weights were positive, so the positive or negative difference between the previous incongruent and congruent trials was always applied in the same direction but was scaled by the weight.

Two examples of the participant-specific models are displayed in Fig 4A, illustrating how the three internal states differentially affect RT in individual participants. The top panel shows the fitted exponential curve and the indicator function for the task type. The middle panels show the three internal states' evolution over the 540 trials. Finally, the bottom panels show the RT overlaid with the predicted RT from the model. To better see the model prediction of RT, Fig 4B shows scatter plots for the two participants, separately showing the data points used for training and testing the model. Overall, we fitted a participant-specific dynamic state-space model which could successfully capture a large portion of the variability of the RT for all participants, even though the factors driving RT could vary in each individual.

Groups of EEG features relate to each internal state. Using the estimated internal states identified for each participant, we asked "Does activity in groups of EEG features relate to each internal state?" Therefore, we generated a neural model (defined by a GLM) using features of the recorded EEG to predict the internal states. Even though the EEG was recorded before and after the distractor, we chose to focus on the EEG data during the 1400 ms prior to the distraction presentation, during the first delay period, because this could be considered the working memory maintenance period of the trial, independent of the transient response to the distractor and recovery of the working memory representation. After processing the epoched EEG data into a matrix of Phase-Locking Values (PLV) for every pair of sensors for each of the five different frequency bands (theta, alpha, low beta, high beta, and gamma), we extracted relevant regional features from the matrix. We grouped the electrode channels into different regions which included: left-frontal, right–frontal, central, left–temporal, right–temporal, left–parieto–occipital, right–parieto–occipital. Specifically, we created a set of Within Region features (by taking the mean of all PLV connections within a specific region) and Between Region features (by taking the mean of all PLV connections between two specific regions). For each participant, we extracted 140 EEG features for all 540 trials.

To identify the groups of EEG features related to each internal state, we first reduced the number of extracted EEG features used in the neural model. Using the feature selection algorithm (detailed in the methods section), we found 43 features that produced the best neural model prediction, across all participants, for each state. Once the final sets of features were selected, we fitted three separate GLMs to estimate each internal state using their respective EEG feature sets (Eqn 9). For the neural model, we labelled the weights on the EEG features as γ in order to differentiate them from the weights of the behavioral model, β.

Fig 5A shows the percentage of EEG features selected from each of the five frequency bands, for each state. Overall, the largest number of selected features was found in the gamma band. We identified groups of EEG features

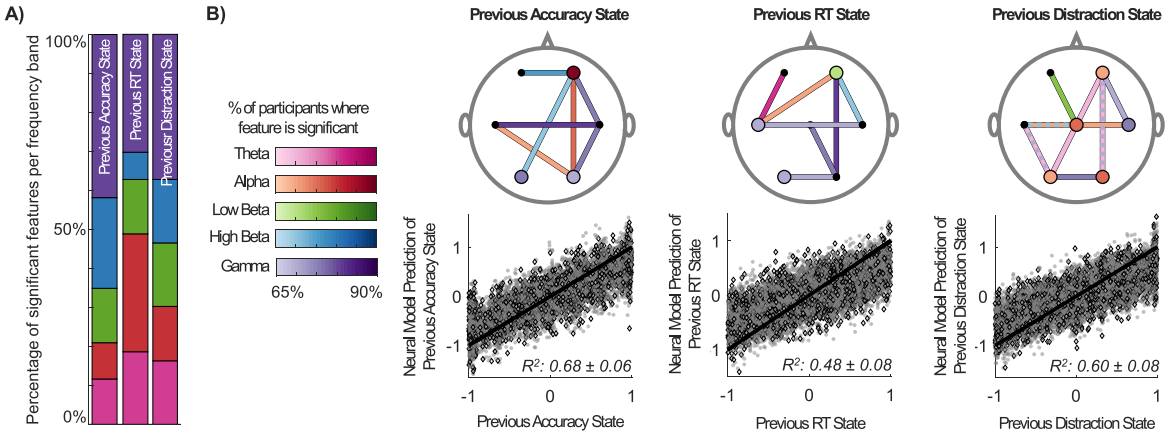

Fig. 5. A) Distribution of the features selected in each frequency band for each internal state. The color to denote each frequency band is the same as in B (Theta is pink, Alpha is red, Low Beta is green, High Beta is blue, and Gamma is purple). B) The features that were significant in over 65% of participants. A feature was considered to be significant if the resulting feature-specific p-value was less than 0.05 from the GLM (i.e. β was significantly different from zero). The plots are shown in the transverse plane and the hemispheres are not flipped. The color of the feature shows the percentage and the frequency band. The Within Region features are shown as colored circles with a black outline. The Between Region features are shown as a colored line with two small black dots at either end. A dotted line shows the feature is present in two different frequency bands. The scatter plots show the performance of the neural model in predicting the internal states. The training and testing data points are denoted by the grey circles and grey diamonds outlined in black, respectively. The solid black line indicates perfect correlation (i.e. the $y = x$ line)

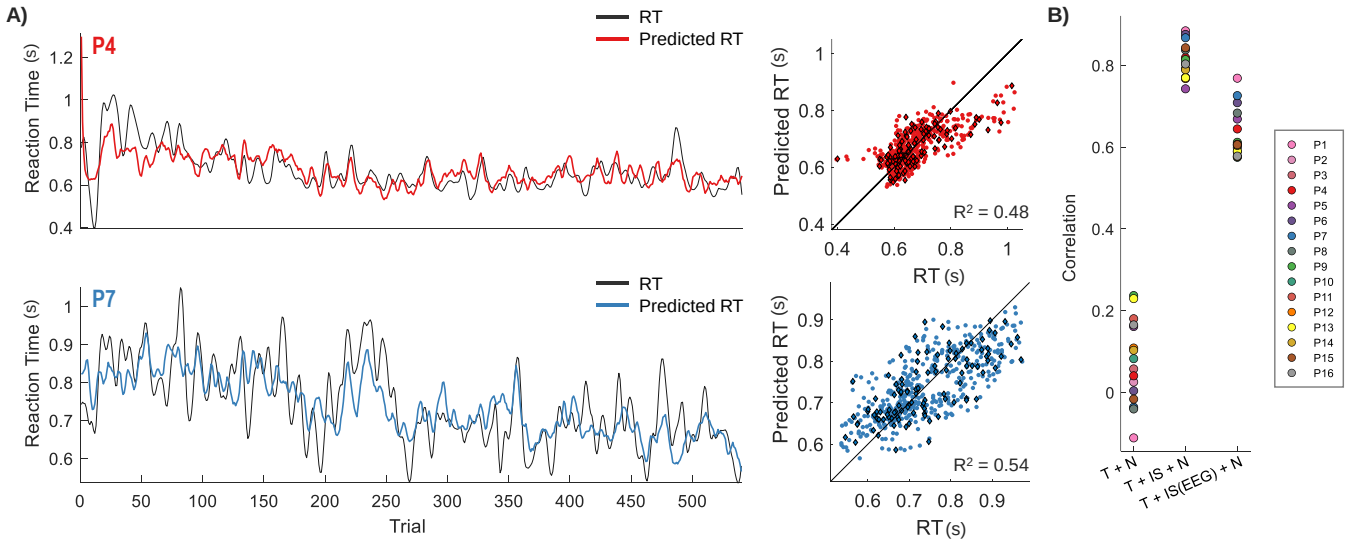

Fig. 6. A) A comparison of the RT and the predicted RT using the estimated internal states from the EEG features. For the scatter plots, the training and testing data points are denoted by the colored circles and colored diamonds outlined in black, respectively. The solid black line shows perfect correlation (i.e. the $y = x$ line) B) An extension to Fig 3A which shows the testing correlation for the dynamical model (T + IS + N) when the states were estimated using the EEG features (T + IS(EEG) + N). T = Task, IS = Internal States estimated from behavioral model, IS(EEG) = Internal States estimated from neural model, N = noise.

for each state, by selecting features that were consistently significant across participants. Specifically, for each feature, we calculated the number of participants for which that feature-specific p-value was significant (< 0.05) from the participant-specific neural models. Fig 5B shows, for each state, the features that were significant in over 65% of participants. Below the EEG features for each state is a scatter plot, for all participants, comparing the predicted internal state estimated from the neural model of EEG features to the corresponding state estimated from the behavioral model.

RT can be predicted using EEG features. Next, we asked, "Can RT be predicted using EEG features related to the internal states?" We substituted each of the internal states estimated from the EEG features in Eqn 9 into the behavioral model in Eqn 3 to predict the RT, for each trial, for each person. Fig 6A shows both the time series responses and scatter plots of the RT compared to the predicted RT using the EEG features, for Participants 4 and 7. Fig 6B shows how the model performance, quantified using correlation, changed if we substituted our internal states from the behavioral model with the estimated internal states using the EEG features (IS(EEG)). Over all participants, the drop in model performance was small and therefore showed that internal states could be related to neural activity measured using EEG. Furthermore, these results showed that this activity could predict a large portion of variability in RT, both within and across individuals.

Weights of individual EEG features modulate linearly with the weight of the internal state for predicting RT. Finally, we asked "Are their correlations between the participant-specific weights of a state in the behavioral model and the weights of a corresponding EEG feature in the neural model?" For this analysis, we focused only on the fitted weights (β and γ), which were fixed, constant, parameters in the model for each participant. Specifically, we identified the strongest linear relationships between the magnitude of the weights of the internal states of the behavioral model ($|\beta|$), and the weights of a single EEG feature in the neural model ($|\gamma|$) (Fig 7). The aim was to better characterize the nature of the individual differences in internal states and their neural bases.

We identified seven EEG features in which, across all 16 participants, the weights determined from the neural model strongly correlated ($R^2 > 0.4$) with the weights of the internal states determined from the behavioral model.

The plots shown Fig 7 can be interpreted based on the direction of the correlation. If the correlation was positive, then, as the internal state weighed into the behavior more (i.e. increase in weight along the x-axis), the EEG feature weight for the internal state prediction also increased (i.e. increase in weight along the y-axis). However, if the correlation was negative, then, as the internal state weighed into the behavior more, the opposite occurred and the EEG feature weighed into the internal state less. Generally, across all three internal states, we observed a positive correlation between the contribution of the internal states in predicting RT, and the resulting magnitude of the EEG feature weight from the neural model for predicting the internal state.

Interestingly, for the Previous Accuracy State, we observed a different relationship for the left parieto – occipital gamma activity versus right fronto – parietal gamma connectivity. Overall, the more that participants actively remembered past errors, the more we observed right fronto – parietal gamma connectivity contributing to the prediction of the Previous Accuracy State, which weighed into RT. For example, P4 highly weighed previous accuracy in the behavioral model while P7 did not, and this was reflected in the weight of right fronto – parietal gamma connectivity in the neural model. The opposite trend oc-

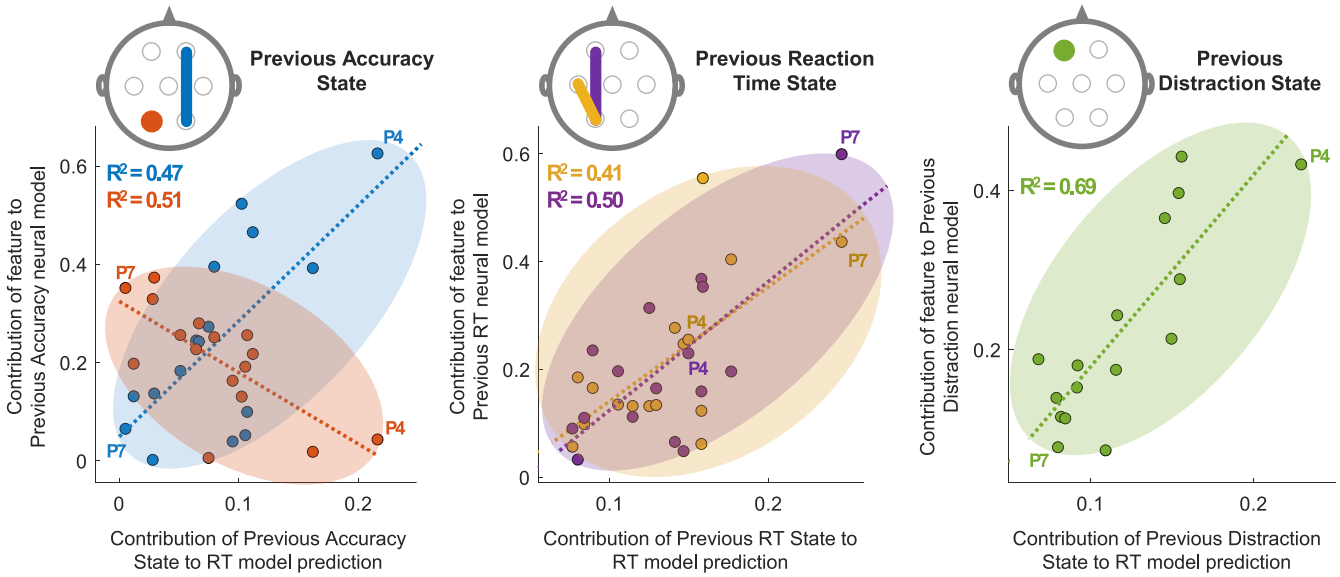

Fig. 7. The highest linear relationships between the weights of the internal states for the behavioral model (β_x) and the weights of the EEG features for the neural model (γ), for each of the three states. We show only the features that produced a $R^2 > 0.4$. For each scatter plot, the color of the dots representing all 16 participants matches the color of the feature shown on the head illustration which are shown in the transverse plane and the hemispheres are not flipped. The dotted line shows the fitted regression line. All these EEG features are in the gamma band, except for the temporal – parietal connection (Previous RT State), which is in the alpha band.

curred with the left parieto – occipital gamma activity. For P7, who barely weighed previous accuracy in predicting RT, the left parieto – occipital gamma weight from the neural model was high, while P4's was low.

For the Previous RT State, the two strongest linear relationships were positive and found in the left fronto – parietal gamma and left temporo – parietal alpha connections. In other words, as the EEG functional connectivity of these two pairs of left-hemisphere regions weighed into the Previous RT State more, we observed participants were more likely to maintain their current trend of increasing or decreasing RT across trials. For example, P7 weighed the previous RT the highest, and, correspondingly, both left-hemisphere connection weights were the largest. We observed a similar trend for P4, even though the weights for both the behavioral and the neural model were not as large.

Finally, the largest R^2 value (0.69) observed reflected the relationship between the Previous Distraction State and left frontal gamma activity. For this state, since the correlation was positive, the more that participant's RT was affected by distractors, the more that left frontal gamma activity weighed into predicting the Previous Distraction State.

Discussion

The current study suggests a new perspective on behavioral and neuroimaging data related to experimentally controlled factors, and illustrates the importance of considering individual differences in dynamic internal states related to strategy, attention and motivation. Previous work on the present dataset (7) revealed that attentional capture by no-longer relevant information was associated with lower posterior alpha power, and that such capture was stronger when spatial relations rather than retinotopic locations were maintained in working memory, as indicated by both ERP magnitude and behavioral effects. The current results indicated, however, that this group effect of the experimental manipulation was small compared to variability in behavior and neural activity within and across individuals. This variability, however, was not noise. It was highly predictable. In particular, three states were found to be associated with task performance across individuals.

First, the Past Accuracy State reflected the influence of errors committed on previous trials. Our findings of right fronto-posterior couplings associated with this state are consistent with previous findings in which errors resulted in greater top-down, proactive control of information processing and response inhibition, mediated in part by right prefrontal cortex, in order to reduce the influence of irrelevant information (7, 10, 11, 15, 16). Following errors, trial-by-trial adjustments were implemented, more so by some participants than others, and appeared to be a major determinant of inter-individual variability in behavioral performance.

Second, the Previous RT State and its associated EEG activity appeared to reflect carry-over effects from one trial to the next regarding information of processing speed, or perhaps attentional arousal and task engagement. Here, in contrast to the Past Accuracy state, left gamma fronto-parietal and alpha parieto-temporal couplings were predominantly involved in predicting the Previous RT State and, thus, RT. Activity and connectivity in the alpha and gamma bands have previously been associated with working memory maintenance and information processing (17, 18). Since P4 and P7 displayed similar accuracy levels in the working memory task, but different degrees of association between this left hemisphere EEG connectivity and RT, the activity identified in the current analysis is likely not directly related to working memory processes.

Further research will be needed, with source localization, to better understand the contribution of the Previous Reaction Time State and its associate neural activity.

Third, the Previous Distraction State referred to the distraction elicited by the incongruence between the hemifield of the distractor and the hemifield of the working memory test, relative to when the elements were congruent (i.e., displayed in the same hemifield). Our previous work (7) revealed a facilitating effect on task performance, on average in the group analysis, when the distractor and the subsequent working memory test were displayed in the same hemifield. Conversely, when the hemifields of the distractor and of the working memory test were different, decreased performance was observed. In the current study, the Previous Distraction State indicated the extent to which an individual's performance on previous trials was affected by the congruence of the distractor and test stimuli. Additionally, the state was associated with left frontal gamma activity and predicted the extent to which a participant's reaction time was affected by congruence on future trials. As with the other internal states, the degree to which the Previous Distraction State and its associated neural activity affected future RT was again highly variable across participants. Despite this variability, the Previous Distraction State coefficient was positive in all participants, consistent with the previous findings in the group analysis. The current analysis, however, adds additional information that is important to understand individual differences in this kind of distraction effect. The distractor color was relevant in a different task that the participants also performed. The Previous Distraction State indicates how much the participant's distraction in previous trials predicts their RT in a current trial. That is, the contribution of the state indicates how much the individual's tendency to be distracted by those stimuli consistently lingered from trial to trial. The left frontal activity, thus, could reflect the degree to which the participants were thinking about the rules of the tasks as it related to the distractors versus focusing only on the spatial working memory stimuli. Thus, again, the current analysis revealed factors affecting behavior and neural activity during the experimental task that are highly variable both within and across individuals. In this case the state may be related to strategy or meta-cognitive processes in order to stay focused on the current task.

Overall, the current study showed the promise of a dynamic systems modeling approach for understanding individual differences in cognitive control. A typical approach to understanding an individual's cognitive strengths and weaknesses compares overall performance in a task that, for example, challenges selective attention versus overall performance in a task that challenges learning from feedback, or working memory capacity. The cognitive abilities of clinical populations have often been assessed in a similar manner. The method demonstrated here could provide a much more sensitive and specific measure of both trait-like and state-dependent cognitive abilities in both individuals and groups. For example, previous research has indicated that sensitivity to reward (or loss) appears to be a trait-like aspect of individual differences in cognitive performance, related to dopamine genotype (19). An individual's sensitivity to reward and their control over reward-related behavior, however, can also vary within an individual across time based on moment-to-moment changes in various contextual factors (20). Susceptibility to distraction is also thought to be somewhat trait-like (21) although it can change with sleep deprivation (22), age (23), learning (24), and other factors. While many task performance measures have poor test-retest reliability (25), the coefficients identified using our modeling approach may be more reliable measures of individual differences, because they measure specific factors that feed into performance. Additionally, our dynamic systems modeling approach could also be applied in the same individuals across multiple tasks and across testing sessions. This would provide critical information to evaluate whether an individual who was, for example, more sensitive to distraction than their peers in a given task was consistently more sensitive across time and experimental contexts. The identification of neural features underlying susceptibility to distraction, or feedback sensitivity, etc., would also provide model-driven targets for training or neuromodulation interventions for improving performance (26, 27).

Materials and Methods

Participants. In total, twenty-six participants were recruited to complete the task. Each participant reported normal or corrected-to-normal vision and gave written informed consent approved by the Institutional Review Board of Johns Hopkins University. In the original study by our group (7), we excluded seven participants from analysis because of excessive EEG artifacts (< 70% of epochs after preprocessing), and/or incorrect trials (< 60% accuracy on the task), and/or technical difficulties. For this work, we excluded an additional three participants because a substantial number of trials did include recorded EEG data. As a result, the recorded data from sixteen right-handed participants (fourteen females, mean age 20.9 ± 2.8 years) was used in this analysis. Please refer to (7), for EEG ERP and time-frequency analysis of this dataset.

Working Memory Task. Participants completed a value-driven attention capture (VDAC) working memory (WM) task to test their ability to ignore a previously learned distractor, which was no longer relevant. For each participant, a session consisted of a training task to associate a target color with a reward, and then the WM task with that target color acting as a distractor to test the effect of the association in another context (Fig 8). During the training phase, participants performed a visual search task which consisted of 240 trials. After a fixation cross was displayed, six circles with different colors were presented (colors: pink, orange, yellow, light blue, black, and either red or green). The participants were asked to report the line orientation (vertical or horizontal) within the target circle via a button press. Targets were defined as a red or a green circle, of which only one was presented on each trial. The participants had 1000ms to respond, otherwise, the trial ended. Reward feedback was given on trials with correct and fast responses (less than 1000ms) which included the reward on the current trial, and the total accumulated reward so far. For their assigned color target (either red or green, counterbalanced across participants), participants received $0.25 on 80% of the correct trials and $0.10 on 20% of the correct trials. The unrewarded color was always followed by $0.00 and the total earned from previous trials.

Then, the participant was told that the color was no longer relevant. During the VDAC WM test phase, participants performed a spatial WM task. The trial began with a black fixation

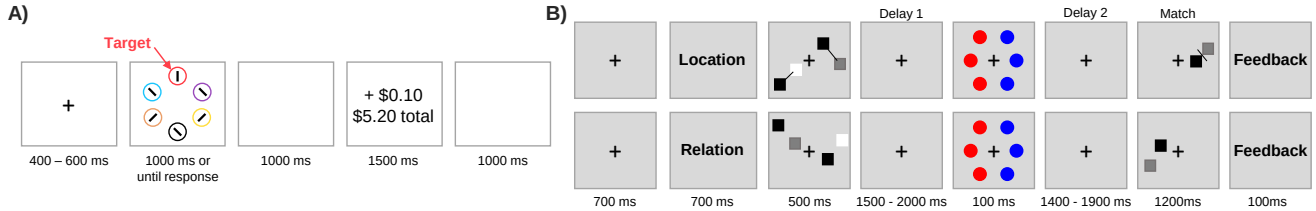

Fig. 8. A) A schematic of the reward training task. B) Trial schematics showing the VDAC WM task for both the Location and Relation Trials, see (7) for additional details.

cross, and then a cue showed which type of task the current trial would be. Specifically, the word "Location" and "Relation" cued that the participants were to remember a particular location (i.e. Location trial) and the relative spatial relationship between the items (i.e. Relation trial), respectively. Four squares, which could be black, gray, or white, were displayed so that two squares of different luminances appeared in each hemifield. After a jittered Delay 1 period (1500 – 2000 ms), six colored distractors, three in each hemifield, were displayed for 100ms. The distractors in each hemifield were either red or green, which were the previously rewarded or non-rewarded colors, or blue which was a novel color. Following another jittered delay period (Delay 2: 14000 – 1900 ms), two test squares in either the left or right hemifield were presented, and the participant had 1200ms to respond. Finally, feedback with the word "correct", "incorrect", or "too slow" was displayed on the screen.

For the Location trials, participants were instructed to draw an imaginary line between the squares in each hemifield and then maintain the spatial coordinates of those two lines during the two delay periods. During the testing period, participants determined whether the test squares were "straddling" the imaginary line formed by the initial two squares in that hemifield.

For the Relation trials, participants were told to encode and maintain the relative vertical positions of the two squares in each hemifield. For example, "was the black square above or below the white square?" During the testing period, participants determined whether the two squares had the same relative positions as the initial squares in that hemifield. For both the Location and Relation trials, participants responded by pressing either a button for a "match" response or another for a "non-match" response.

In total, the participants completed 540 trials, where 270 Location trials and 270 Relation trials were pseudo-randomly presented. The session was divided into nine runs of 60 trials, with two additional training sessions of the visual search task included between runs 3 and 4 and between runs 6 and 7, to reinforce the learned reward-color association.

Pre-processing Behavioral Data. The first step in developing the behavioral models was to pre-process the RT data. First, on trials where the participant took longer than 1200 ms to answer, the trial was considered incorrect and RT was listed as 0. This occurred in an average of 1% of trials across participants. In order to improve the fit of the models to predict RT, we estimated what their RT might have been by interpolating between the one trial before and the one after the timed-out trial. The final pre-processing step was to filter the RT timeseries by using a smoothing spline (smoothing factor of 0.15).

Developing Behavioral Models of RT. To predict RT using behavioral data for each participant, we used a general linear model (GLM). To assess the performance of the models, we computed the Pearson Correlation Coefficient, which is a measure of linear correlation between two variables (in this case, the predicted RT and recorded RT). The coefficient ranged between +1 (positive linear correlation) and -1 (negative linear correlation), where 0 represented no correlation.

Model: Task + Noise (T + N). We defined our initial model (Eqn 2) of RT to be a function of the Task Type, Hemifield, Congruent Trial, and Incongruent Trial. First, the Task Type, $s_t(t)$, was an indicator function where 0 and 1 represented the type of trial (location task vs. relation task), respectively. Next, the Hemifield indicator function, $s_h(t)$, identified the hemifield of the test stimulus (right vs left) on each trial. Finally, two separate indicator functions were used to specify the Congruent Trials, $s_c(t)$, and Incongruent Trials, $s_i(t)$.

We divided the trials into one training set (80%) and one testing set (20%). Specifically, to generate the testing set, every 5th trial was removed from the total of 540 trials and concatenated. The remaining trials were concatenated and used as the training set to fit the GLM. Using Matlab, we fitted the T + N model using a GLM to predict the RT, for each person. The resulting fitted GLM produced the β's, and the associated p-value for each term of the model, which were an indication of whether the β's were significantly different from zero. Additionally, the β's provided important information about how much that specific term contributed to the prediction of RT. From the results, we found the model did not capture the dynamics of the RT well.

Model: Task Type + Internal States + Noise (T + IS + N). Based on the results of the initial model, we defined a modified model (Eqn 3) which included the initial T + N model, in addition to an exponential trend, and three internal states. State-space models were used to define the three internal states $(x_1(t), x_2(t), x_3(t))$: the Previous Accuracy State (Eqn 4), Previous RT State (Eqn 5), and Previous Distraction State (Eqn 6).

For the Previous Distraction State, we defined t_i to be the previous incongruent trial and t_c to be the previous congruent trial. A congruent or incongruent trial was defined as when the two testing squares appeared in the same or opposite hemifield as the displayed rewarded distractor, respectively.

The evolution of each of the internal states, over the 540 trials, depended on the a's, which could be considered to be the memory in the system. For example, in the Previous Accuracy State, when an incorrect answer was given, the state received a positive unit impulse. If a_1 was small (close to 0), then the response to the impulse decayed quickly. On the other hand, if a_1 was large (close to 1) then the decay occurred slowly over the following trials and could accumulate if several incorrect answers occurred close together. In order to account for the gap in working memory task blocks when retraining the distractor color (after trials 180 and 360), we reset each of the three states back to zero, after those trials.

In total, we had four parameters that needed to be selected: a_e, a_1, a_2, a_3, from Eqns 3-6. Therefore, we used a search-grid to examine different combinations of a values and fitted the GLM model for each iteration. We evaluated the internal state, a's, from 0.01 to 0.99, and the exponential trend, a_e, from 0.5 to 0.9995. For the exponential trend, the initial condition was set to 1. For each iteration of the search grid, we divided up the trials into the same training (80%) and testing (20%) set that was used for the initial behavioral model. The training set was used to fit the GLM, and the testing set was used to test the correlations.

Using a systemic grid-search approach over all the a's, we developed a 4D matrix of root-mean-squared-error (RMSE) values (computed between the predicted RT and the RT training dataset). To find the final model, the minimum RMSE value of the 4D matrix was selected. Then, using the selected final combination of a's, the GLM was fit to identify the β's, but in this iteration, each of the terms of the model was normalized to compare the fitted β's across participants. Overall, this process was repeated sixteen times to identify the best behavioral model for each participant.

EEG Recording and Processing. Besides recording behavior, 32 channels of EEG were recorded using an ActiCHamp System (Brain Products, Munich, Germany) and was referenced to Cz. The session took place in an electromagnetically shielded room to reduce noise in the data. Electrode impedance was kept below 20 kΩ and all EEG electrodes were recorded continuously in DC mode at a sampling rate of 512Hz. The electrodes used in this analysis were Fp1, Fp2, F7, F3, F4, F8, FT9, FC5, FC1, FC2, FC6, FT10, T7, C3, C4, T8, TP9, CP5, CP1, CP2, CP6, TP10, P7, P3, P4, P8, O1, O2.

For each of the 540 trials per person, the raw EEG data was pre-processed using the EEGLAB toolbox (version 14.4.2b) (28) in Matlab2020a. First, the data were bandpass filtered (1Hz – 55Hz) using an FIR filter to remove drift and the 60Hz power line noise. The order of the filter was the value selected automatically by EEGLAB, which was 1650. Next, the filtered EEG was re-referenced to the average. Then, the mean value of each channel was subtracted to ensure zero mean. Subsequently, the artifacts were removed using the automatic continuous rejection in EEGLAB. EEGLAB's default independent component analysis algorithm (29) employed logistic infomax-based ICA (30). Each of the components were plotted as 2-D scalp maps and the components which were associated with eye blinks were selected manually. The selected components were then removed by projecting the sum of selected non-artefactual components back onto the scalp. Next, the clean EEG was bandpass filtered (1650th order FIR filter) into the five different frequency bands: Theta (4Hz – 8Hz), Alpha (8Hz – 12Hz), Low Beta (12Hz – 20Hz), High Beta (20Hz – 30Hz), and Low Gamma (30Hz – 55Hz).

Phase Locking Value (PLV) Matrix Computation. Using the cleaned EEG data, for each trial, we computed five PLV matrices, one per frequency band, that were comprised of nodes (electrode channels) and edge weights (PLV). PLV measured the phase coherence between two signals. For example, the PLV of two identical oscillators was 1 if the phase difference was continually fixed, and was 0 if constantly changing (31).

For this analysis, we computed the PLV matrices from the clean EEG data 1400ms prior to the distractor presentation in the task (during Delay 1). We chose to use this epoch for several reasons. First, this time period could be considered to be the working memory maintenance portion of each trial. Additionally, after the distractor, EEG activity could be less predictive because it could be a reflection of 1) how well the participant was ready for the distraction, and 2) how fast they were able to recover from the distraction.

The first step in computing the PLV value was to convert the entire length of the timeseries into analytic signals using a Hilbert transform (32). The instantaneous phase of the analytic signal, in radians, of electrode channel h was denoted $\phi_h(t)$. Second, we computed the phase difference between channels h and i by

$$\theta_{hi}(t) = (\phi_h(t) - \phi_i(t)) \mod 2\pi. \qquad [7]$$

Then, the initial 10% and final 10% of the timeseries were removed to account for the edge effect from the Hilbert transform. Finally, all pairs of channels were compared against each other via the PLV defined as

$$\mathrm{PLV}_{hi} = \frac{1}{N}\left|\sum_{k=1}^{N} \exp\Big(j\theta_{hi}(k\Delta t)\Big)\right|, \qquad h, i = 1, 2, \ldots, n, \qquad [8]$$

where n was the total number of electrode channels, $j = \sqrt{-1}$ was the imaginary unit, and $\Delta t = \frac{T}{N}$ where T was the timeseries duration and N was the total number of discrete time steps.

PLV Matrix Feature Extraction. Once the PLV matrices were computed for each frequency band, on each trial, for each person, we extracted the relevant features of each matrix. To reduce the number of features of interest, we defined seven regions, which were left–frontal (Fp1, F7, F3), right–frontal (Fp2, F4, F8), central (FC1, FC2, CP1, CP2), left–temporal (FT9, FC5, T7, C3, TP9, CP5), right–temporal (FC6, FT10, C4, T8, CP6, TP10), left–

$$\text{T + N Model: } \log(RT(t)) = \underbrace{\beta_0}_{\text{constant}} + \underbrace{\beta_t s_t(t)}_{\text{Task Type}} + \underbrace{\beta_h s_h(t)}_{\text{Hemifield}} + \underbrace{\beta_c s_c(t)}_{\text{Congruent Trial}} + \underbrace{\beta_i i_t(t)}_{\text{Incongruent Trial}} + \underbrace{N(0,\sigma^2)}_{\text{Noise}} \qquad [2]$$

$$\text{T + was + N Model: } \log(RT(t)) = \underbrace{\beta_0}_{\text{constant}} + \underbrace{\beta_t s_t(t)}_{\text{Task Type}} + \underbrace{\beta_h s_h(t)}_{\text{Hemifield}} + \underbrace{\beta_c s_c(t)}_{\text{Congruent Trial}} + \underbrace{\beta_i i_t(t)}_{\text{Incongruent Trial}}$$
$$+ \underbrace{\beta_e e^{-a_e(t)}}_{\text{Exponential}} + \underbrace{\beta_{x_1} x_1(t)}_{\text{Previous Accuracy State}} + \underbrace{\beta_{x_2} x_2(t)}_{\text{Previous RT State}} + \underbrace{\beta_{x_3} x_3(t)}_{\text{Previous Learned Distraction State}} + \underbrace{N(0,\sigma^2)}_{\text{Noise}} \qquad [3]$$

$$\text{Previous Accuracy State: } x_1(t+1) = \begin{cases} a_{x_1} x_1(t) + 1 & \text{if incorrect answer on trial } t \\ a_{x_1} x_1(t) & \text{if correct answer on trial } t \end{cases} \qquad [4]$$

$$\text{Previous RT State: } x_2(t+1) = a_{x_2} x_2(t) + \text{sign}(RT(t) - RT(t-1)) \qquad [5]$$

$$\text{Previous Distraction State: } x_3(t+1) = \begin{cases} a_{x_3} x_3(t) + (RT(t) - RT(t_c) & \text{if trial } t \text{ is incongruent} \\ a_{x_3} x_3(t) - (RT(t_i) - RT(t) & \text{if trial } t \text{ is congruent} \\ a_{x_3} x_3(t) & \text{if other trial type} \end{cases} \qquad [6]$$

The T + N model tests four different experimentally structured task rules: Task Type, Hemifield, Congruent Trials, and Incongruent trials. Based on the results of the participant-specific fitted models, the Task Type term was significant (p-value < 0.05) in more than 50% of participants. Hemifield, Congruent trials, and Incongruent trials were significant in 25%, 0%, and 0% of participants, respectively. Therefore, to reduce the model complexity of T + IS + N, but still retain the task rules component, the Hemifield, Congruent, and Incongruent terms were removed (shown by the grayed out terms). Additionally, for the Previous Distraction State, the Incongruent and Congruent terms were used to identify t_i and t_c, respectively.

parieto–occipital (P7, P3, O1), and right–parieto–occipital (P4, P8, O2).

In general, we were interested in Within Region and Between Region features. Specifically, to compute the Within Region features, we averaged all the PLV connections within each of the regions defined above. To compute the left–frontal Within Region feature value, we averaged the Fp1 – F7, F7 – F3, Fp1 – F3 PLV connections together. For the Between Region features, the computation was similar except now we computed the average connection between regions. For example, to find the left–frontal to right–frontal connection, we averaged the Fp1 – Fp2, Fp1 – F4, Fp1 – F8, F7 – Fp2, F7 – F4, F7 – F8, F3 – Fp2, F3 – F4, F3 – F8 connections together. For each PLV matrix, we computed all Within Region and Between Region features, for all trials, frequency bands, and participants.

We concatenated all features together to create a 540 (trials) by 140 (EEG feature) matrix, for each participant. In total, there were 35 Within Region features (7 features per 5 frequency bands) and 105 Between Region features (21 features per 5 features bands).

In order to compare the neural models across participants, we normalized the feature matrix using a series of steps. First, each of the 140 features was turned into a new quantized vector (ranging from -3 to 3), by creating a histogram with 7 bins from the timeseries. For example, the feature vector time points that fell in the smallest value bin were set equal to -3. Then, the feature vector time points that fell into the second smallest bin were set equal to -2. This process continued until we reached the time points in the feature vector contained in the largest value bin, and the new feature vector time points was set to 3. Then, we applied the same smoothing spline (smoothing factor = 0.15) to the newly computed quantized feature vector. Finally, we normalized the smoothed quantized feature vector to ensure that the range of the timeseries was between -1 and 1. This process was applied to each feature vector, for all participants.

Neural Model and Feature Selection. The purpose of the neural model was to predict the internal states by using a combination of EEG features. We applied an additional GLM which was defined as

$$\hat{x}(t) = \sum_{i=1}^{43} \gamma_i F_i(t) \qquad [9]$$

where $\hat{x}(t)$ was the estimated internal state on trial t, and γ_i was the weight multiplied by each of the EEG feature vectors, $F_i(t)$. We included an additional step for fitting the neural model which was to quantize, smooth, and normalize the individual states using the same methodology described before for the EEG features.

In order to prevent overfitting, we chose to use only 10% of the number of trials in the training dataset, which was 43. Therefore, we applied the following feature selection methodology for each state. Similar to the behavioral model, the same trial indices were used to divide up the data into testing and training datasets. Our overall aim was to find a set of features that produced the smallest prediction error using the training dataset, across all participants.

First, our feature selection algorithm included all 140 features in the GLM prediction. For each person, we systematically fitted 140 separate GLM using all the features except for one and saved the resulting RMSE between the predicted RT and the RT. Then, we identified the feature, that when removed, produced the smallest maximum change in RMSE value, across all participants. Then, that feature was removed from the pool of features for the next search iteration. Subsequently, using the remaining 139 features, one feature at a time was systematically removed, and then, again, we removed the feature which produced the smallest maximum change in RMSE across all participants. This process continued until only 43 features remained.

In the next step, we further refined the feature selection by swapping out the features. First, we saved the mean RMSE of the model, across all participants, using the current feature selection. Next, for the first participant, we systematically switched out each of the remaining features with all the features that had been removed. Therefore, to test all combinations, a total of 4,171 feature swaps were completed and the resulting RMSE was saved. We repeated this feature swap for all participants, and saved the resulting RMSE, which created a 3D matrix [Participant $\times$ features in $\times$ features out]. Then, by taking the mean (across the Participants) of the RMSE metric, we identified the minimum index (swapping an "in" feature for an "out" feature) of the matrix. If that swap produced a mean RMSE value across participants smaller than what was previously saved, then the feature swap iteration continued. If not, then the algorithm was stopped, and the last set of features was selected as the final set used for the neural model.

Using the sets of selected EEG features for each state, we computed a final neural model to predict each internal state, for each person. Using the output of the GLM, we extracted the weights in front of each EEG feature, γ, and its associated p-value.

Predicting RT using estimated internal states from EEG features. To determine if RT could be predicted using EEG, we substituted the estimated internal states, using the EEG features, from the neural model (Eqn 9) for the original internal states (Eqn 4, 5, 6) of the behavioral model. Then, we re-fit the GLM for each person and computed the correlation values between the predicted RT and RT.

Identifying EEG features weights which modulate with the magnitude of the individual internal state weights for predicting RT. As a final analysis, we wanted to identify EEG features which modulated with the weight of the internal states identified from the behavioral model. Therefore, we identified the strongest linear relationships between the fitted weights of the internal states from the behavioral model (β_x) and the weights of the EEG features in the neural model (γ). The following process was completed for all three internal states, but, for this example, we used the Previous Accuracy State, x_1. For Participant 1, we plotted the absolute value of the Previous Accuracy State weight, $|\beta_{(x_1,P_1)}|$, from their behavioral model against the absolute value of the neural model weight for the first selected EEG feature, $|\gamma_{(F_1,P_1)}|$. This resulted in one point in the $|\beta_{x_1}|$ vs $|\gamma_{F_1}|$ space. Then, we repeated this process for all participants, P. Next, we fitted a linear model to the 16 data points, which was generally described by

$$|\gamma_{(F,P)}| = c_0 + c_1|\beta_{(x,P)}| \quad \text{for } \mathrm{P} = [1, 2, \ldots, 16] \qquad [10]$$

where $x = [1, 2, 3]$ was the state, $F = [1, 2, \ldots, 43]$ was the EEG feature, and P was the 16 participants. The intercept and slope of the regression line were c_0 and c_1, respectively. From the linear model, we extracted the R^2 value. We repeated this process for all 43 EEG features, for each state, and identified which neural features modulated with the contribution of the states to the RT prediction. The features which showed the largest linear trend ($R^2 > 0.4$) for each of the three internal states are shown in Fig 7.

ACKNOWLEDGMENTS. The authors would like to thank Kara Blacker and Brian Anderson for their work on the original experimental study and Michelle DiBartolo for her work developing the modeling approach using a different data set. This work was supported by the Johns Hopkins Science of Learning Research Grant and NIH/NINDS T32 NSO70201 (Interdisciplinary Training in Biobehavioral Pain Research)

1. AD Baddeley, G Hitch, Working memory in *Psychology of learning and motivation.* (Elsevier) Vol. 8, pp. 47–89 (1974).
2. A Baddeley, Working memory. *Curr. biology* **20**, R136–R140 (2010).
3. M D'Esposito, BR Postle, The cognitive neuroscience of working memory. *Annu. review psychology* **66**, 115–142 (2015).
4. LQ Uddin, Bring the noise: reconceptualizing spontaneous neural activity. *Trends Cogn. Sci.* (2020).
5. I Dinstein, DJ Heeger, M Behrmann, Neural variability: friend or foe? *Trends cognitive sciences* **19**, 322–328 (2015).
6. RL Goris, JA Movshon, EP Simoncelli, Partitioning neuronal variability. *Nat. neuroscience* **17**, 858–865 (2014).

7. T Hinault, K Blacker, M Gormley, B Anderson, S Courtney, Value-driven attentional capture is modulated by the contents of working memory: An eeg study. *Cogn. Affect. & Behav. Neurosci.* **19**, 253–267 (2019).
8. BA Anderson, A value-driven mechanism of attentional selection. *J. vision* **13**, 7–7 (2013).
9. BA Anderson, The attention habit: How reward learning shapes attentional selection. *Annals new York Acad. Sci.* **1369**, 24–39 (2016).
10. FM Stoll, V Fontanier, E Procyk, Specific frontal neural dynamics contribute to decisions to check. *Nat. communications* **7**, 1–14 (2016).
11. HA ElShafei, L Fornoni, R Masson, O Bertrand, A Bidet-Caulet, What's in your gamma? activation of the ventral fronto-parietal attentional network in response to distracting sounds. *Cereb. Cortex* **30**, 696–707 (2020).
12. P Sacré, et al., Risk-taking bias in human decision-making is encoded via a right–left brain push–pull system. *Proc. Natl. Acad. Sci.* **116**, 1404–1413 (2019).
13. P Sacré, et al., The influences and neural correlates of past and present during gambling in humans. *Sci. reports* **7**, 1–9 (2017).
14. P Sacré, et al., Lucky rhythms in orbitofrontal cortex bias gambling decisions in humans. *Sci. reports* **6**, 1–10 (2016).
15. S Wu, et al., The neural dynamic mechanisms of asymmetric switch costs in a combined stroop-task-switching paradigm. *Sci. reports* **5**, 1–11 (2015).
16. KZ Xu, et al., Neural basis of cognitive control over movement inhibition: human fmri and primate electrophysiology evidence. *Neuron* **96**, 1447–1458 (2017).
17. J Daume, T Gruber, AK Engel, U Friese, Phase-amplitude coupling and long-range phase synchronization reveal frontotemporal interactions during visual working memory. *J. Neurosci.* **37**, 313–322 (2017).
18. T Hinault, M Kraut, A Bakker, A Dagher, S Courtney, Disrupted neural synchrony mediates the relationship between white matter integrity and cognitive performance in older adults. *Cereb. Cortex* **30**, 5570–5582 (2020).
19. T Hahn, et al., Association between reward-related activation in the ventral striatum and trait reward sensitivity is moderated by dopamine transporter genotype. *Hum. brain mapping* **32**, 1557–1565 (2011).
20. FX Castellanos, EJ Sonuga-Barke, MP Milham, R Tannock, Executive function: is there a central executive? *Trends Cogn. Sci.* **3**, 117–123 (2006).
21. S Forster, N Lavie, Establishing the attention-distractibility trait. *Psychol. science* **27**, 203–212 (2016).
22. ME Stepan, KM Fenn, EM Altmann, Effects of sleep deprivation on procedural errors. *J. Exp. Psychol. Gen.* **148**, 1828 (2019).
23. O Slobodin, H Cassuto, I Berger, Age-related changes in distractibility: developmental trajectory of sustained attention in adhd. *J. attention disorders* **22**, 1333–1343 (2018).
24. S Chang, CA Cunningham, HE Egeth, The power of negative thinking: Paradoxical but effective ignoring of salient-but-irrelevant stimuli with a spatial cue. *Vis. Cogn.* **27**, 199–213 (2019).
25. C Hedge, G Powell, P Sumner, The reliability paradox: Why robust cognitive tasks do not produce reliable individual differences. *Behav. research methods* **50**, 1166–1186 (2018).
26. KT Jones, DJ Peterson, KJ Blacker, ME Berryhill, Frontoparietal neurostimulation modulates working memory training benefits and oscillatory synchronization. *Brain research* **1667**, 28–40 (2017).
27. KT Jones, EL Johnson, ME Berryhill, Frontoparietal theta-gamma interactions track working memory enhancement with training and tdcs. *Neuroimage* **211**, 116615 (2020).
28. A Delorme, S Makeig, Eeglab: an open source toolbox for analysis of single-trial eeg dynamics including independent component analysis. *J. Neurosci. Methods* **134**, 9–21 (2004).
29. S Makeig, AJ Bell, TP Jung, TJ Sejnowski, , et al., Independent component analysis of electroencephalographic data. *Adv. neural information processing systems*, 145–151 (1996).
30. AJ Bell, TJ Sejnowski, An information-maximization approach to blind separation and blind deconvolution. *Neural computation* **7**, 1129–1159 (1995).
31. JP Lachaux, E Rodriguez, J Martinerie, FJ Varela, , et al., Measuring phase synchrony in brain signals. *Hum. Brain Mapp.* **8**, 194–208 (1999).
32. IW Selesnick, The design of approximate hilbert transform pairs of wavelet bases. *IEEE Transactions on Signal Process.* **50**, 1144–1152 (2002).